

Data Repository Item

“How big was the Chesapeake Bay Impact? Insight from numerical modeling”

By Gareth S. Collins and Kai Wünnemann

In our paper we present the results of a single simulation of the Chesapeake Bay impact event. To understand the variability of our results and the sensitivity to model parameters, and to justify our selection of a best-fit case, we present here some alternative simulations and elaborate on the details of our modeling.

Description of constitutive model (adapted from Collins et al., 2004)

The complexity involved with accurately simulating impact events to late stages resides in how to prescribe the appropriate yield strength for a given cell of material in the target. Rock mechanics experiments show that the critical stress at the onset of failure is a function of confining pressure, temperature, strain rate, porosity and sample size. Furthermore, brittle materials show two distinct types of failure mechanism: tensile failure and shear failure. The following discussion details the constitutive model used in the simulations presented in this paper. The algorithm stems largely from the work of Boris Ivanov (for example, Ivanov et al., 1997), supplemented by recent collaboration between Boris Ivanov, Jay Melosh and the authors. This description was adapted from Collins et al. (2004).

Shear Failure

iSALE treats the target as an elastic-plastic solid. This means that the rheologic stress in a given cell is linearly related to the strain, for stresses below the yield stress or *strength*. Above this yield stress the material behaves plastically, in the sense that deformation is permanent, and the stress is limited by the yield stress. The procedure for implementing this scheme is to compare an invariant measure of stress in a cell with the prescribed yield stress. The stress invariant used in iSALE is the second invariant of the deviatoric stress tensor J_2 , given by:

$$J_2 = \frac{1}{6} \left[(\sigma_{e1} - \sigma_{e2})^2 + (\sigma_{e2} - \sigma_{e\theta})^2 + (\sigma_{e\theta} - \sigma_{e1})^2 \right], \quad (\text{A1})$$

where σ_{ei} are the elastic principal stresses in cylindrical coordinates. The elastic principal stresses are computed from the elastic deviatoric stresses, which are defined by the elastic

deviatoric strain components. These are updated each time step by first assuming that all deformation is elastic. If J_2 exceeds the square of the yield strength Y , then shear failure has occurred: the updated elastic deviatoric stress components (and deviatoric elastic strains components) must be reduced to the yield envelope by multiplying by the factor $Y/\sqrt{J_2}$. The remaining strain (the difference between the elastic deviatoric strain components before and after the yield correction is applied) is the plastic strain.

To approximate the effect of pressure on yield strength for intact rock Y_i , we use a smooth approximation to experimental data first defined by Lundborg (1968):

$$Y_i = Y_0 + \frac{\mu_i P}{1 + \mu_i P / (Y_M - Y_0)}, \quad (\text{A2})$$

where Y_0 is the shear strength at zero pressure, μ_i is the coefficient of internal friction and Y_M is known as the von Mises plastic limit of the material.

For completely fragmented rock material, we use a Coulomb dry-friction law (Stesky et al., 1974). In this case the yield strength is given by:

$$Y_d = \mu_d P, \quad (\text{A3})$$

where μ_d is the coefficient of friction for the damaged material. This relationship is only valid for confining pressures where $Y_d < Y_i$; at pressures above this the shear strength follows the same pressure dependence given by Equation A2, regardless of damage.

For partially fragmented material a quantity called “damage” D is defined, which takes a value of between 0 for completely undamaged, to 1 for totally damaged material. The damage quantity may then be used to define intermediate yield strengths according to the equation (after Ivanov et al., 1997):

$$Y = (1 - D)Y_i + DY_d. \quad (\text{A4})$$

Damage may be accumulated due to shear deformation or tensile failure. Here we separate the two mechanisms and define the total damage D as the sum of the tensile damage D_t , which will be discussed in the next section, and the shear damage D_s . Following the scheme of Johnson and Holmquist (1993), among others, we define the shear damage as the

integrated plastic strain ε_{tot} divided by the accumulated plastic strain at the point of failure ε_f , which is known to be a function of pressure, temperature and material type:

$$D_s = \min\left(1, \frac{\varepsilon_{tot}}{\varepsilon_f}\right). \quad (\text{A5})$$

The integrated plastic strain is calculated by adding an invariant measure of the plastic strain accumulated in the time step each cycle. Thus, the total plastic strain ε_{tot} is given by a sum over all time-steps $n = 1$ to n_{tot} :

$$\varepsilon_{tot} = \sum_{n=1}^{n_{tot}} \dot{E}_n \Delta t_n, \quad (\text{A6})$$

where Δt_n is the duration of the n^{th} time step and \dot{E}_n is an invariant measure of the plastic strain rate in that step, defined in cylindrical coordinates by:

$$\dot{E}_n = \left(\frac{1}{6} \left[(\dot{\varepsilon}_{1,n} - \dot{\varepsilon}_{2,n})^2 + (\dot{\varepsilon}_{2,n} - \dot{\varepsilon}_{\theta,n})^2 + (\dot{\varepsilon}_{\theta,n} - \dot{\varepsilon}_{1,n})^2 \right] \right)^{1/2}, \quad (\text{A7})$$

where $\dot{\varepsilon}_{i,n}$ are the principal plastic strain rate components for the n^{th} cycle.

To define the plastic strain required for complete failure, we adopt the philosophy presented in Evans and Kohlstedt (1995), where shear failure occurs within one of three regimes: brittle, semi-brittle and plastic, depending on the confining pressure (see Fig. 1). For low confining pressures, where the strength of the damaged material is less than that for intact specimens ($Y_d < Y_i$), the plastic strain at failure rises from 0.01 at zero pressure, to 0.05 at the brittle-ductile transition pressure p_{bd} . In this regime rock failure is by discrete brittle failure along microcracks. Failure occurs after minimal plastic strain and the strength drop due to damage is significant. Hence, strong strain localization is expected. In contrast, for very large confining pressures, where the pressure is greater than twice the shear strength ($p > 2Y$), we define the plastic strain at failure to rise abruptly from 0.1 at the brittle-plastic transition pressure p_{bp} to 1 at twice the brittle-plastic transition pressure. In the semi-brittle regime, which lies in the pressure range $p_{bd} < p < p_{bp}$, we define the plastic strain at failure to rise linearly from 0.05—0.1. This reflects the deformation regime which includes both brittle fracture and ductile flow. Rock deforming in this regime will show signs of brittle failure, however, the damage has no effect on the yield strength.

The shear strength of rock materials also depends on temperature (see for example, Jaeger and Cook, 1969). As the material approaches the melting temperature the shear strength drops off to zero at the melting temperature. We approximate this behavior using the simple relationship (after Ohnaka, 1995):

$$Y_t = Y \tanh\left(\xi\left(\frac{T_m}{T} - 1\right)\right), \quad (\text{A8})$$

where T and T_m are the ambient and melt temperature respectively and ξ is a material constant.

The complete shear strength algorithm is as follows. The shear strength of the material in the cell is determined based on the current pressure, temperature and damage. The stress in the cell is calculated assuming that all the strain can be accommodated elastically. If this stress exceeds the yield strength, the elastic stresses and strains are reduced and the remaining strain is accommodated plastically. This plastic strain is recorded and used to determine the shear damage by dividing it by the plastic strain at failure, which is a function of pressure. The total damage in the cell to be used in the subsequent time step is this shear damage plus any tensile damage that may have accumulated. Tensile failure was not modeled in our simulations of the Chesapeake Bay impact.

Acoustic Fluidization

To facilitate complex crater collapse we also include the effect of transient, high-frequency pressure oscillations in the target surrounding the impact point. These pressure fluctuations modify the frictional strength of the damaged target by temporarily reducing the overburden pressure; hence, allowing temporally- and spatially-localized slip between rock fragments. The time- and space-averaged result of these small-scale slip events is that the rock mass takes on a fluid-like rheology from a macroscopic point-of-view. This process is known as acoustic fluidization (Melosh, 1979). The acoustic fluidization algorithm implemented in iSALE follows the “block-model” approximation of Ivanov and Kostuchenko (1997). The algorithm is discussed in detail in Melosh and Ivanov (1999). Briefly, the sub-crater fractured target material is assumed to comprise of large rock blocks surrounded by a matrix of much smaller fragments. The vibrational velocity of these blocks is assumed to be a fraction (c_{vib})

of the maximum particle velocity U_{max} in the shock wave that engulfs the block zone, and is assumed to decay exponentially with time t after the shock-wave passes:

$$v_{vib} = \min(200, c_{vib} |U_{max}| e^{t/T_{dec}}), \quad (\text{A9})$$

In this expression T_{dec} is the characteristic decay time of the vibrations (an input parameter); the minimum ensures that the vibrational velocity in a cell never exceeds a prescribed limit, taken to be 200 m/s. The pressure associated with these vibrations in a given cell is taken to be

$$p_{vib} = \rho c_s v_{vib}, \quad (\text{A10})$$

where ρ is the bulk density of the cell and c_s is the bulk sound speed of the cell. The yield strength of a cell within the block zone is modified by this vibrational pressure according to the expression:

$$Y_{vib} = \mu_d (p - p_{vib}) + \rho v_{lim} \dot{\epsilon}, \quad (\text{A11})$$

where v_{lim} is the kinematic viscosity of the acoustically fluidized cell and $\dot{\epsilon}$ is an invariant measure of the strain rate in the cell (c.f. Eq. A7). The yield strength in a cell is set equal to Y_{vib} if this is less than the standard yield strength (given by Eq. A4).

Model parameters for simulations of Chesapeake Bay impact

Table DR1 and Figures DR1-DR3 present the constitutive model parameters used in the five simulations of the Chesapeake Bay impact presented here. The results of Model 1 are presented in the paper, in Figure DR4, and in an animation accompanying this document. Models 2-5 are presented only as animations accompanying this supporting material. We present these alternative models to illustrate the variability in our results and our reasons for considering Model 1 to be the best fit to observational constraints.

All models employed identical strength models for the granite basement. Model 3 used an alternative damage model to all other models; in this case the plastic strain at failure ϵ_f (Eq. A5) was reduced relative to the other models (see Fig. DR3).

All models employed identical strength models for the intact sediments (see Figs. DR1 and DR2). In Model 1 (our best-fit model), Model 2 and Model 4 we used a very low coefficient of friction for the damaged sediments ($\mu_d = 0.01$; pink dashed line in Figs DR1 and DR2); in this case the damaged sediments were almost strengthless. In Model 3 and 5 a higher value was used for the coefficient of friction for the damaged sediments.

Discussion

Figure DR4 shows the results from Model 1. The figure supplements Figure 2 in the paper, showing plots of total plastic strain on the left and accumulated damage on the right. The first two time frames ($t = 5$ and 45 s) illustrate the growth of the cavity and the shock-induced damage and deformation in the surrounding target. The later frames illustrate the collapse and infilling of the cavity, and the inward movement of the fluidized sediments. The figure illustrates the tremendous difference between the amount of deformation in the sediments versus the basement rocks in the outer basin. Also evident is the disruptive influence of the ejecta layer as it lands and interacts with the partially shock-damaged sediments.

The difference between Model 1 and Model 2 illustrates the effect of varying the impactor size. That is, all model parameters in Model 2 are the same as in Model 1 except for impactor diameter (and appropriately-scaled acoustic fluidization parameters), which is 4.6 km in Model 2, and 3.2 km in Model 1. In this case, uplift of the basement beneath the transient crater rim occurs much further out than the ~ 20 km inner ring observed at Chesapeake Bay. Furthermore, the inner basin is significantly deeper than in Model 1, and the sedimentary unit is much more deformed. This places a good constraint on the impactor diameter, provided that the weak strength model used for the sediments is applicable. In other simulations (not shown), in which the sedimentary unit was assumed to be stronger, inward collapse of the sediments was prevented by inherent strength and the uplifted rim of basement.

Model 3 illustrates an alternative dynamic model for the formation of the inner ring that is analogous to the suggested model for peak-ring formation at Chicxulub (Collins et al., 2002). In this model, the basement rock becomes damaged at a smaller strain; consequently, the target is weaker and the acoustically-fluidized zone beneath the growing crater is larger and persists for longer. This leads to a much larger transient crater begin formed, which then collapses more spectacularly. The central uplift in this model overshoots the pre-impact target surface before collapsing back downward and outward. A topographic ring feature forms inside, but concentric to, the main crater rim when the collapsing central uplift material collides with the inwardly collapsing transient crater rim. Thus a topographic high is evident in the basement rocks at the same approximate location as the inner ring at Chesapeake Bay (~ 20 km radius); however, the deformation in the basement rocks exterior to this is not at all consistent with interpretations of the seismic data over this part of the Chesapeake Bay crater. Furthermore, unlike the interpreted cross-section of the Chesapeake Bay crater, the floor of the crater in the inner basin does not lie below the level of the basement floor in the outer basin. We therefore do not favor a dynamic formation model of this type.

Model 4 illustrates the effect of considering a water layer above a thinner sediment layer as opposed to the single, thicker sedimentary layer used in Model 1. The final crater structure is very similar to the simpler two-layer model. We interpret this to mean that our combined model of the water layer and sedimentary sequence was not a drastic oversimplification of the target model. We do not believe that the complex dynamics involved in the late stage infilling of the inner basin in the three-material model is very accurate, and are much more confident in the two-material model in this regard. This is because iSALE does not do an adequate job of modeling averaged material properties in mixed cells where all three materials (water, sediments and basement) are present.

We performed Model 5 to test whether the resurgence of a water layer could drive the movement of sediments back into the inner basin even if the sediments were a bit stronger than Model 1 suggests. However, we found that even using a quite low coefficient of friction for the damaged sediments (0.2), the water resurgence could not force back into the crater the large volume of sediments required to fill the inner basin. This result gives us more confidence that a very weak overall strength of the sedimentary unit is indeed required to explain the formation of the Chesapeake Bay impact crater.

References

- Collins, G.S., Melosh, H.J., and Ivanov, B.A., 2004, Modeling Damage and deformation in impact simulations: *Meteoritics & Planetary Science*, v. 39, no. 2, p. 217–231.
- Collins G. S., Melosh H. J., Morgan J. V., Warner M. R. 2002. Hydrocode simulations of Chicxulub Crater collapse and peak-ring formation, *Icarus*, **157**: 24-33.
- Evans B. and Kohlstedt D. L. 1995. Rheology of Rocks, In: T. J. Ahrens (Ed.) *Rock Physics and Phase Relations: A handbook of physical constants*, AGU, Washington, pp. 148-165.
- Ivanov B. A., Deniem, D. and Neukum, G. 1997. Implementation of dynamic strength models into 2D hydrocodes, Applications for atmospheric break-up and impact cratering, *International Journal of Impact Engineering*, 17: 375-386.
- Ivanov B. A. and Kostuchenko V. N. 1997. Block oscillation model for impact crater collapse (abstract #1655), 27th Lunar and Planetary Science Conference. CD-ROM.
- Johnson G. R., Holmquist T. J. (1993) An improved computational constitutive model for brittle materials. In: Schmidt SC, Shaner JW, Samara GA, Ross M, editors, High-Pressure Science and Technology - 1993, AIP Press, Woodbury NY. pp. 981-984

- Jaeger J. C. and N. G. W. Cook 1969. *Fundamentals of Rock Mechanics*. Chapman and Hall, London.
- Lundborg N. 1968. Strength of rock-like materials. *Int. J. Rock Mech. Min. Sci.* **5**: 427-454.
- Melosh H. J. 1979. Acoustic Fluidization: A new geologic process? *J. Geophys. Res.*, **84**: 7513—7520.
- Melosh H. J. and Ivanov B. A. 1999. Impact crater collapse, *Ann. Rev. Earth Planet. Sci.* **27**: 385-415.
- Ohnaka M. 1995. A shear failure strength law of rock in the brittle-plastic transition regime. *Geophys. Res. Lett.* **22**: 25-28.
- Stesky, R.M., Brace, W.F., Riley, D.K., and Robin, P.Y.F., 1974, Friction in faulted rock at high temperature and pressure: *Tectonophysics*, v. 23, p. 177–203.

Chesapeake Bay Strength Models

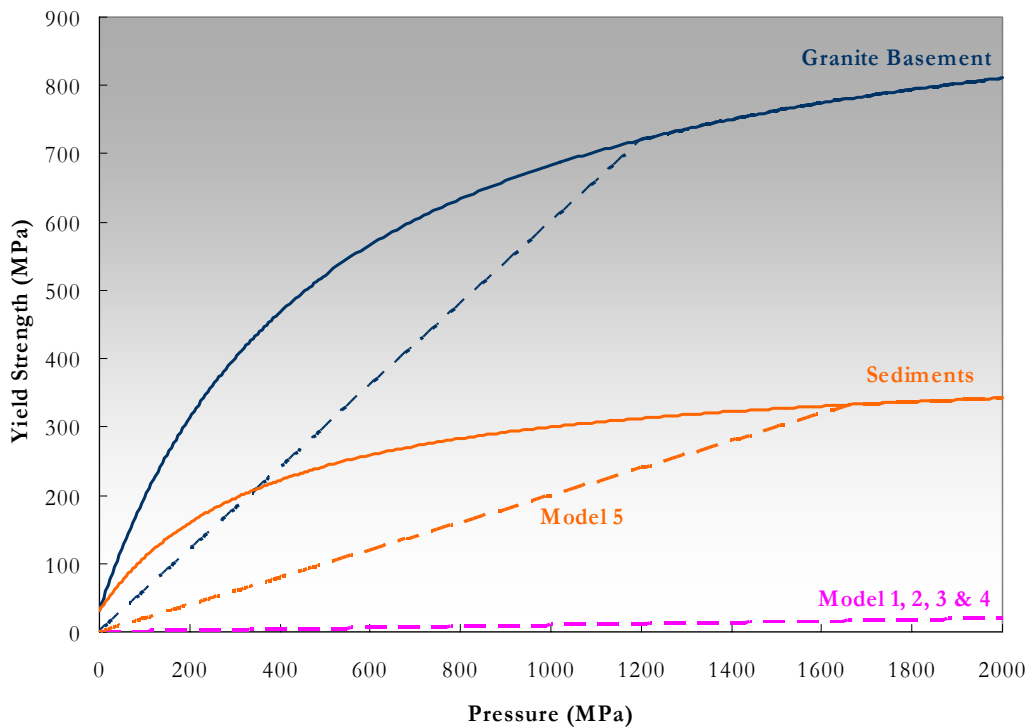


Figure DR1 (above)

Figure DR2 (below)

Chesapeake Bay Strength Models (Sediments-detail)

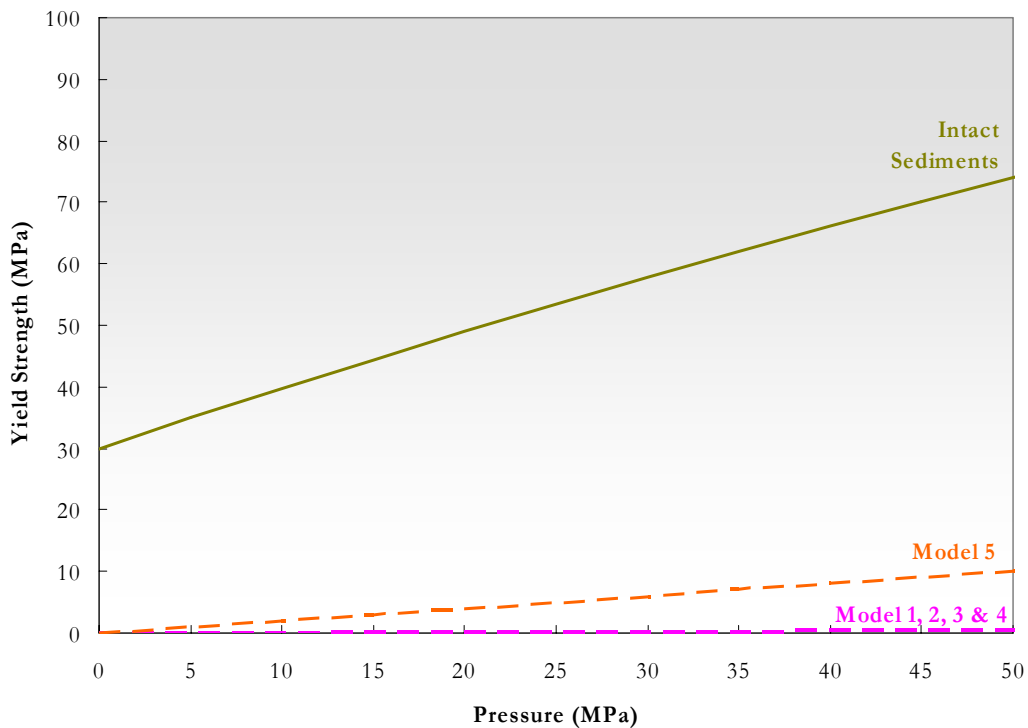


Figure DR3

Chesapeake Bay Damage Models (Granite Basement)

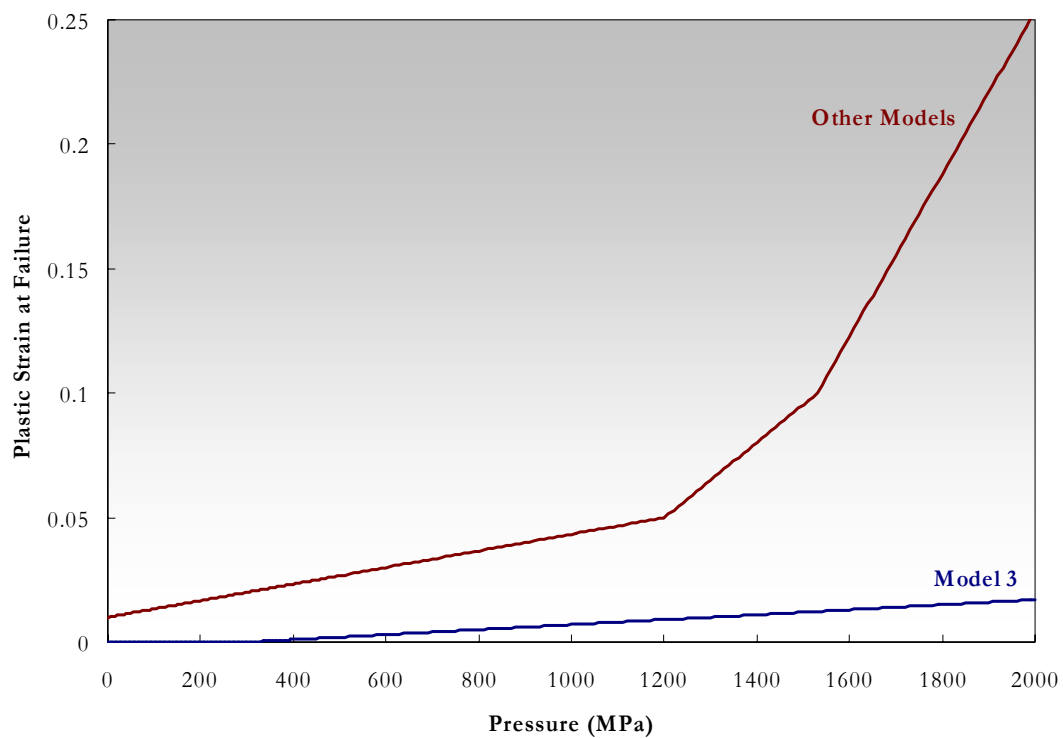


Figure DR4: Numerical simulations results from Model1 (see also Figure 2 in paper)

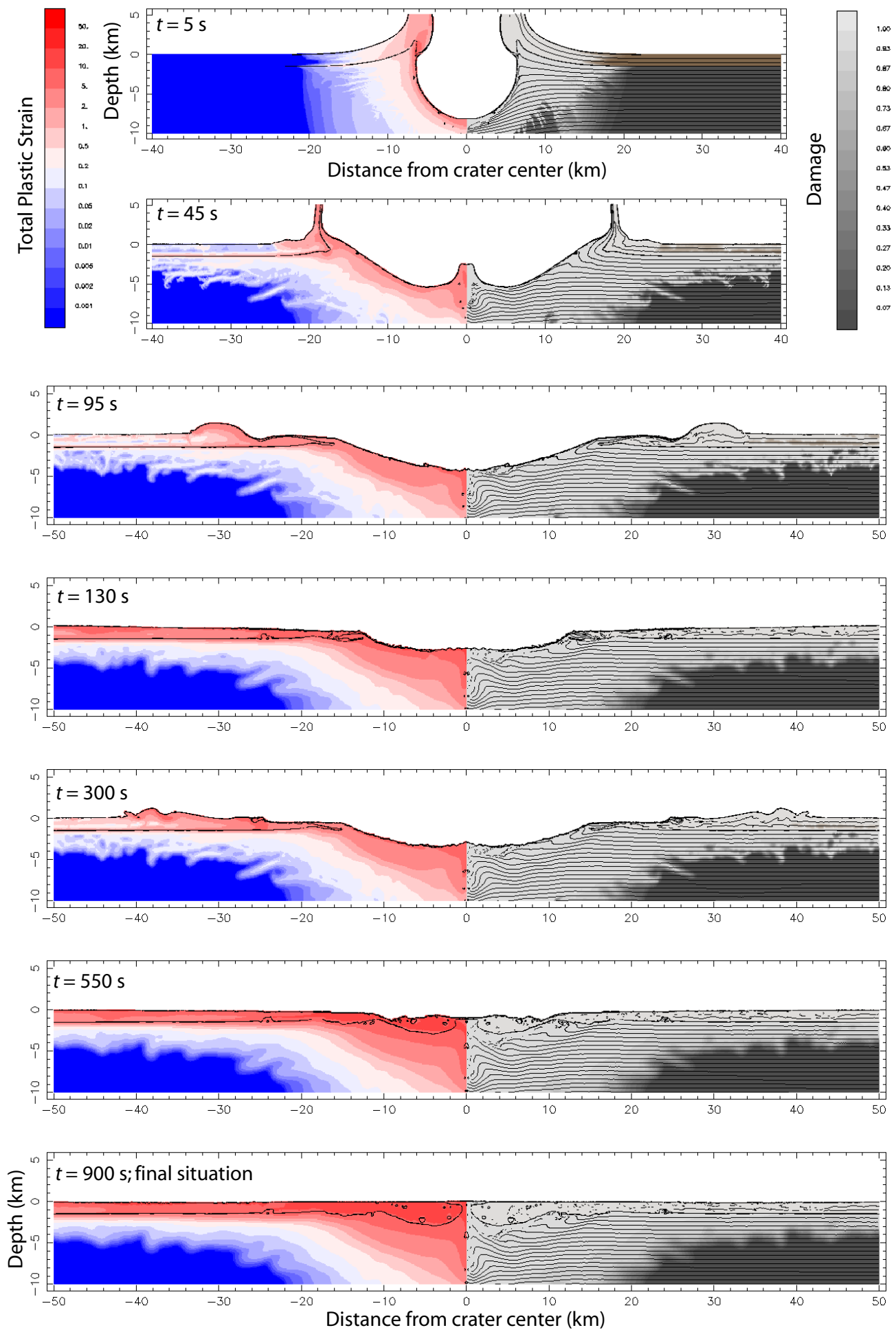


Table DR1: Model parameters used in simulations of Chesapeake Bay impact

Symbol	Definition	Model 1		Model 2		Model 3	
		Basement	Sediments	Basement	Sediments	Basement	Sediments
L	Impactor diameter (km)	3.2		4.6		4.6	
v_i	Impact velocity (km/s)	17.8		17.8		17.8	
ρ_i	Impactor density (kg/m ³)	2680		2680		2680	
T_{dec}	Decay time of acoustic vibrations (s)	38.4		54.0		54.0	
v_{lim}	Kinematic viscosity of acoustically fluidized region (m ² /s)	80000		112500		112500	
ρ	Reference density (kg/m ³)	2680	1970	2680	1970	2680	1970
Y_0	Cohesion (Yield strength at zero pressure; MPa)	30	30	30	30	30	30
Y_m	von Mises plastic limit (theoretical yield strength at infinite pressure; GPa)	1.5	0.4	1.5	0.4	1.5	0.4
μ_i	Coefficient of internal friction	2.0	1.0	2.0	1.0	2.0	1.0
μ_d	Coefficient of friction	0.6	0.01	0.6	0.01	0.6	0.01
T_m	Melt temperature (°K)	1500	1500	1500	1500	1500	1500
ξ	Thermal softening parameter	1.2	1.2	1.2	1.2	1.2	1.2
p_{bd}	Brittle-ductile transition pressure (GPa)	1.20	N/A ¹	1.20	N/A	N/A	N/A
p_{bp}	Brittle-plastic transition pressure (GPa)	1.53	N/A	1.53	N/A	N/A	N/A

¹ Plastic strain at failure assumed to be 5-8% and independent of pressure for sediments ($\epsilon_f = 0.05-0.08$)

Symbol	Definition	Model 4			Model 5		
L	Impactor diameter (km)	3.2			3.2		
v_i	Impact velocity (km/s)	17.8			17.8		
ρ_i	Impactor density (kg/m ³)	2680			2680		
T_{dec}	Decay time of acoustic vibrations (s)	38.4			38.4		
ν_{lim}	Kinematic viscosity of acoustically fluidized region (m ² /s)	80000			80000		
		Basement	Sediments	Water	Basement	Sediments	Water
ρ	Reference density (kg/m ³)	2680	1970	976.	2680	1970	976.
Y_0	Cohesion (Yield strength at zero pressure; MPa)	30	30	0.	30	30	0.
Y_m	von Mises plastic limit (theoretical yield strength at infinite pressure; GPa)	1.	0.4	0.	1.	0.4	0.
μ_i	Coefficient of internal friction	2.0	1.0	0.	2.0	1.0	0.
μ_d	Coefficient of friction	0.6	0.01	0.	0.6	0.2	0.
T_m	Melt temperature (°K)	1500	1500	273	1500	1500	273
ξ	Thermal softening parameter	1.2	1.2	N/A	1.2	1.2	N/A
p_{bd}	Brittle-ductile transition pressure (GPa)	1.20	N/A ¹	N/A	1.20	N/A	N/A
p_{bp}	Brittle-plastic transition pressure (GPa)	1.53	N/A	N/A	1.53	N/A	N/A